Velocity of SuperDARN echoes at intermediate radar ranges

Alexander Koustov[1], Michael R Luciuk[2], Robert G Gillies[3], Sydney Ullrich[2], Bion Larson[4], Kathryn A Mcwilliams[5], and Marina Schmidt[2]

[1]University of Saskatchwean
[2]U of Saskatchewan
[3]U of Alberta
[4]U of Saskacthewan
[5]University of Saskatchewan

November 22, 2022

Abstract

The study investigates the relationship between SuperDARN HF radar velocities detected at intermediate ranges of 600-100 km from the radar and the plasma drift. Two approaches are implemented. First, a three-hour interval of SuperDARN Rankin Inlet (RKN) radar measurements and Resolute Bay incoherent scatter radar RISR-C measurements in nearly coinciding directions are investigated to show that 1) HF echoes with low velocities (less than 200 m/s) are often detected when drifts are in excess of 1000 m/s, 2) high-velocity HF echoes from the E region have velocities somewhat below the expected values of the ion-acoustic speed of the plasma and the HF velocity does not show a tendency for an increase at the largest drifts, 3) for E region echoes, 12 MHz velocities are slightly larger than those at 10 MHz, and 4) It often occurs that 12 MHz echoes are received from the electrojet heights while 10 MHz echoes are received from the F region heights so that the observed velocities are quite different with the latter reflecting the drift of the plasma. In the second approach, velocities of 10 and 12 MHz RKN echoes are compared for a large data set comprising several months of observations to show that occurrence of 12 MHz low-velocity echoes is fairly common (up to 25% of the time) whenever the flows are fast. Under this condition, the SuperDARN cross polar cap potential is underestimated by ~4 kilovolts.

Velocity of SuperDARN echoes at intermediate radar ranges

Alexander V. Koustov
Department of Physics and Engineering Physics, University of Saskatchewan, Saskatoon, Saskatchewan, Canada
e-mail: sasha.koustov@usask.ca

Michael R. Luciuk
Department of Physics and Engineering Physics, University of Saskatchewan, Saskatoon, Saskatchewan, Canada
e-mail: mrl280@mail.usask.ca

Robert G. Gillies
Department of Physics and Astronomy, University of Calgary, Calgary, Alberta, Canada
e-mail: rgillies@ucalgary.ca

Sydney Ullrich
Department of Physics and Engineering Physics, University of Saskatchewan, Saskatoon, Saskatchewan, Canada
e-mail: sju861@mail.usask.ca

Bion Larson
Department of Physics and Engineering Physics, University of Saskatchewan, Saskatoon, Saskatchewan, Canada
e-mail: bil104@mail.usask.ca

Kathryn A. McWilliams
Department of Physics and Engineering Physics, University of Saskatchewan, Saskatoon, Saskatchewan, Canada
e-mail: kathryn.macwilliams@usask.ca

Marina Schmidt
Department of Physics and Engineering Physics, University of Saskatchewan, Saskatoon, Saskatchewan, Canada
e-mail: marina.schmidt@usask.ca

Correspondence to: A.V. Koustov, sasha.koustov@usask.ca

Key points

- SuperDARN velocities 600-1000 km from radar are often low despite fast plasma drift
- Up to 25% of high-latitude vectors in SuperDARN maps can be underestimated
- High-speed *E* region echoes have velocities below the ion-acoustic speed

Keywords: SuperDARN radars; irregularity velocity, electron drift, *E* region, ion-acoustic speed, incoherent scatter radar RISR-C

Abstract

The study investigates the relationship between SuperDARN HF radar velocities detected at intermediate ranges of 600-100 km from the radar and the $\mathbf{E}\times\mathbf{B}$ plasma drift. Two approaches are implemented. First, a three-hour interval of SuperDARN Rankin Inlet (RKN) radar measurements and Resolute Bay incoherent scatter radar RISR-C measurements in nearly coinciding directions are investigated to show that 1) HF echoes with low velocities (less than 200 m/s) are often detected when $\mathbf{E}\times\mathbf{B}$ drifts are in excess of 1000 m/s, 2) high-velocity HF echoes from the *E* region have velocities somewhat below the expected values of the ion-acoustic speed of the plasma and the HF velocity does not show a tendency for an increase at the largest $\mathbf{E}\times\mathbf{B}$ drifts, 3) for *E* region echoes, 12 MHz velocities are slightly larger than those at 10 MHz, and 4) It often occurs that 12 MHz echoes are received from the electrojet heights while 10 MHz echoes are received from the *F* region heights so that the observed velocities are quite different with the latter reflecting the $\mathbf{E}\times\mathbf{B}$ drift of the plasma. In the second approach, velocities of 10 and 12 MHz RKN echoes are compared for a large data set comprising several months of observations to show that occurrence of 12 MHz low-velocity echoes is fairly common (up to 25% of the time) whenever the flows are fast. Under this condition, the SuperDARN cross polar cap potential is underestimated by ~4 kilovolts.

Plain Language Summary

This paper compares velocities measured by the SuperDARN radar at Rankin Inlet (RKN) with plasma flow measurements made by the incoherent scatter radar in about the same directions. The study focuses on RKN ranges where ionospheric echoes can arrive not only from the *F* region (~300 km) but also from the much lower *E* region (~100 km). We investigate one event when the flow was fairly uniform, roughly along the radar beams and fast with plasma drifts up to 1 km/s. We show that despite fast-flowing plasma, RKN occasionally detects low-velocity echoes not related to the plasma drift. Traditional *E* region echoes with velocities consistent with the ion-acoustic speed were also observed. However, for a number of ranges the 12 MHz low-velocity echoes were received from the *E* region heights while 10 MHz echoes, with the velocity close to the plasma drift, were received from the *F* region heights. The velocity ratio in these cases was on the order of 3. We then show that such a situation may occur up to 25% of the time for the RKN radar. In these cases, SuperDARN cross polar cap potential can be underestimated by 5-10 kV.

Introduction

The Super Dual Auroral Radar Network (SuperDARN) high-frequency (HF) radars are widely used for ionospheric convection mapping (Chisham, 2007; Nishitani et al., 2019). The radars measure Doppler velocity of coherent echoes resulting from electromagnetic waves scattered by decameter ionospheric irregularities. Because such irregularities are stretched along the magnetic field lines, the radar waves have to propagate almost perpendicular to the magnetic field lines for the returned signals to be detected. For SuperDARN, the radio wave orthogonality can be achieved at both *E* region (~100 km) and *F* region (~300 km) heights. Typically, *E* region echoes are observed at short ranges of 300-700 km (radar range gates of 2-10) while *F* region echoes are observed at far ranges of 700-1500 km (range gates of 10-30). A SuperDARN range gate typically extends 45 km in distance from the radar, or in range, and the distance to the start of the first range gate is typically 180 km. Besides direct radio wave propagation to the ionospheric irregularities SuperDARN can detect echoes through the so-called "one and a half hop" (1&1/2-hop) propagation mode when radio waves travel to the ionosphere, are refracted forward towards the ground, reflected forward from the ground towards the ionosphere and backscattered from ionospheric irregularities at much larger ranges (beyond range gate 30). For SuperDARN, the 1&1/2-hop propagation mode can be supported through ray path bending in both the *E* and *F* regions.

From the beginning of the SuperDARN project, it was anticipated that the *E* region echoes would negatively affect the quality of the convection maps because *E* region velocities are not necessarily the $\mathbf{E}\times\mathbf{B}$ plasma drift component, at least for observations roughly along the $\mathbf{E}\times\mathbf{B}$ flow (Greenwald et al., 1995). The original design of the SuperDARN network was to merge Doppler plasma drift velocity components from two independently measured directions (Greenwald et al., 1995). Accordingly, the radars were constructed in pairs with overlapping fields-of-view with beam crossings at over the horizon ranges (which is ~1200 km for the *E* region electrojet heights). However, the problem with *E* region echo contamination persisted because of the 1&1/2-hop propagation mode occurrence, albeit in limited amounts (Chisham & Pinnock, 2002; Lacroix & Moorcroft, 2001; Milan et al., 1997).

Introduction of the Potential Fit approach (Ruohoniemi & Baker, 1998) made the problem more acute although not acknowledged. This is because this approach, originally and for many years, used velocity measurements from all ranges, including short-range gates heavily contaminated by the *E* region echoes. To overcome the difficulty, one can filter out all the data at short ranges, but, to the best of our knowledge, this is seldom done. One of the problems is that typical ranges of *E* region echoes must be firmly established. No real effort has been done in this regard so far. In part, this is because the boundary is very dynamic. In the case of a strong sporadic *E* layer presence, HF echoes can come from *E* region heights at the smallest range gates of 0-1. For a highly depleted ionosphere, however, *E* region echoes can come from far-range gates, up to 20 (ranges of ~1100 km), see for example the lines of near orthogonality for the Stokkseyri SuperDARN radar beams in Gorin et al. (2012). Working with the elevation angle data can potentially identify *E* region echoes but handling elevation data in routine SuperDARN measurements has proven to be a challenging task (Ponomarenko et al., 2018). Recently, Thomas and Shepherd (2018), while creating a new statistical model of high-latitude convection acknowledged the fact that SuperDARN velocities at ranges <800 km and >2000 km may be an underestimation of the true plasma drift component and simply did not consider data in these domains for each radar. This certainly addressed the problem but not entirely because the plasma drift underestimation can occur at ranges 800-2000 km owing to the occurrence of *E* region echoes (Lacroix and Moorcroft, 2001).

One can alternatively think of establishing empirically the relationship between the *E* region HF velocity and the $\mathbf{E}\times\mathbf{B}$ velocity. This approach had been successfully implemented in STARE measurements at very high frequencies (VHF), e.g., Nielsen & Schlegel (1985). Unfortunately, the amount of high-quality data for the case of SuperDARN is extremely limited (Davis et al., 1999; Gillies et al., 2018; Koustov et al., 2005). Several studies used the velocity of SuperDARN echoes at far ranges as a proxy for the $\mathbf{E}\times\mathbf{B}$ vector at shorter ranges thus assuming ionospheric flows to be uniform (Gorin et al., 2012; Makarevich et al., 2004; Milan & Lester, 1998; Yakymenko et al., 2015). These studies did not conclude on the relationship quantitatively. Comparisons of HF and VHF velocities at large flow angles showed that, typically, the velocity of HF echoes is smaller than that of the VHF echoes although cases with much larger HF velocity were identified as well (Koustov et al., 2001; 2002; Makarevich et al., 2002). Thus, none of the comparisons performed so far arrived at a well-specified relationship.

Establishing the relationship between the velocity of *E* region electrojet echoes and the $\mathbf{E}\times\mathbf{B}$ velocity is an important issue for the plasma physics of irregularity formation because resolving it allows one to understand the mechanisms of decameter irregularity excitation (e.g., Fejer & Kelley, 1980; Schlegel, 1996). Despite decades of efforts, the question continues to be unresolved. For a long time, it has been believed that for observations at large azimuthal angles with respect to the $\mathbf{E}\times\mathbf{B}$ flow or slow drifts below the ion-acoustic speed of the *E* region plasma C_S, when primary Farley-Buneman (FB) irregularities are not generated, HF/VHF radars would measure the cosine component of the plasma drift (Nielsen & Schlegel, 1985; Uspensky et al., 2006). This notion, accepted for VHF observations (Nielsen & Schlegel, 1985), seems to not applicable at HF (Koustov et al., 2001; 2005; Makarevich et al., 2004). The HF velocity was found to be a fraction of the drift component and can be of opposite the polarity when a radar is looking almost perpendicular to the plasma drift (Makarevich et al., 2004).

For observations along the plasma flow direction and $\mathbf{E}\times\mathbf{B}$ drift speeds faster than the ion-acoustic speed C_S, the expectation is that the velocity of electrojet irregularities is “saturated” at C_S (Nielsen & Schlegel, 1985). This has been traditionally attributed to the nonlinear effects in the development of the FB plasma instability (Fejer & Kelley, 1980). Several SuperDARN publications reported the occurrence of such echoes (e.g., Gillies et al. (2018) and references therein) with the speeds being close to C_S. One inconsistency is that for fast $\mathbf{E}\times\mathbf{B}$ drifts, which are typical for high-latitude plasma flows, the ion-acoustic speed values are expected to rise well above 400 m/s, reaching 600 m/s (Gorin et al., 2012). In addition, it is not clear if one can use the traditional isothermal approach to the analysis of the FB plasma instability (Dimant & Sudan, 1995; 1997). If the FB instability is saturated at C_S, the measured velocity should be in excess of 400 m/s and should increase with the $\mathbf{E}\times\mathbf{B}$ speed. Various SuperDARN publications, however, point at velocities being in the range below 300-400 m/s (e.g., Gillies et al., 2018; Makarevich, 2008; 2009; 2010). This inconsistency can be reconciled by assuming that the velocity of the *E* region echoes for fast flows is a component of the C_S (Bahcivan et al., 2005; 2006), but testing this hypothesis in each specific case requires knowledge of the $\mathbf{E}\times\mathbf{B}$ vector, and these data are usually not available.

Both aspects of E region echo detection with SuperDARN--the relationship of their velocity with the $\mathbf{E}\times\mathbf{B}$ vector and the locations within the SuperDARN FOVs of such echo detection--are still of considerable interest despite the large body of work performed. The progress on both issues has been hindered by the lack of joint E region SuperDARN velocity observatioons with coincident and concurrent $\mathbf{E}\times\mathbf{B}$ drift measurements from other systems, such as incoherent scatter radars (ISRs). In reality, this is a difficult observation to achieve, as ISRs are positioned at far ranges from the SuperDARN radar locations (more than 900 km, range gates >15), where E region echo detection is infrequent. In this study, we attempt to gain knowledge of both the location of occurrence and the velocity components of E region SuperDARN echoes.

2. Coherent echo formation at HF

For a better understanding of the issues addressed in this study, we give a brief description of HF coherent radar signal formation.

HF radio waves transmitted into the ionosphere experience refraction controlled by the electron density distribution in the ionosphere. Generally, 3-D analysis is required, but many major features of HF radio wave propagation at high latitudes can be illustrated by considering a 2-D model of the electron density distribution, changing vertically and with distance from the radar. In a case of smooth spatial variations, such as those in statistical ionospheric models, e.g. E-CHAIM (Themens et al., 2017), the application of Snell's law is straightforward. The high-latitude ionosphere, however, contains inhomogeneities of various scales. They affect radio wave paths locally and can potentially introduce significant deviations of radio wave paths from those expected for a "smooth" ionosphere (Uspensky et al., 1993). Such effects are traditionally ignored in HF propagation analysis because detailed information on localized inhomogeneities is usually not available. In our modeling presented below, we included their effects by introducing a local tilt of an ionospheric layer where refraction occurs, at every step of calculations, and allowing random departures of the tilt from the large-scale density trend given by the E-CHAIM model.

Figure 1 gives an example of HF radio wave tracings in the high-latitude ionosphere applied to the SuperDARN radar at Rankin Inlet (RKN, 62.8° Glat, $-92.1°$ Glon). The direction of beam 5 (azimuth=$-2.4°$) and an operating frequency of 10 MHz were considered. The purpose of the ray tracing here is to identify those parts of the ionosphere where radio waves propagate within $\pm 0.1°$ of orthogonality with the magnetic field so that, if magnetic field-aligned ionospheric irregularities are present, a return signal can be detected. The ACCGMv2 (Shepherd, 2014) magnetic field model was employed. For this specific case, the electron density was assumed to be distributed as given by the E-CHAIM model by Themens et al. (2017) at 19 UT on 6 March 2016 (HF SuperDARN data for his event will be discussed later). Typical densities are $3\times10^{11}\ m^{-3}$ at F region heights and $<1.0\times10^{11}\ m^{-3}$ at E region heights. One can notice a decrease in the F region electron density toward higher latitudes, which is typical for daytime conditions (Themens et al. 2017).

Black/grey lines in Fig.1a are the radar ray paths. The shade of grey helps to delineate the elevation angle of the radar ray path as it is emitted from the radar. The radio waves were launched at elevation angles between 2° and 40° with a $\sim 0.1°$ step, applying Snell's law every 1.5 km along the propagation path. At every step of the Snell's law application, the tilt of the electron density contour was computed from the E-CHAIM model and some deviation from the regular large-scale trend was introduced. Additional random tilts of the layer were assumed to be randomly distributed according to the normal law with the zero average and the $2°$ width. These are arbitrary assumptions. Certainly, stronger allowable tilt deviations from a regular value would provide larger departures of ray trajectories from those given in a "smooth" ionosphere (represented by the E-CHAIM model). White dots along the trajectories denote SuperDARN range gates 0, 10 and 20. Red dots denote SuperDARN range gates 5, 15 and 25. The range gate locations (their nearest edge) were computed by taking into account the radio wave group flight time in the ionosphere.

Figure 1a shows that high-elevation rays (dark grey) reach heights of the *F* region electron density peak and low elevation rays (light grey) occur at the *E* region heights of ~100 km. Yellow marks in Fig. 1a indicate those ranges along each trajectory where the radio waves are within $\pm 0.1°$ of the orthogonality with the magnetic field. Although there is some scatter in the locations of the yellow points in Fig. 1a, two clusters are recognizable. One narrow band is centered just above the 100 km (white) mark at latitudes of $68.2° - 70.9°$ (corresponding to range gates 10-15). Another, a more widespread cloud, occurs between the heights of 200 km and 300 km and at farther latitude/range gates. The pattern of yellow points for the *E* and *F* region heights is reminiscent of the letter "V" rotated by $90°$ clockwise.

Provided the ionospheric irregularities are uniformly filling the entire ionosphere, the two clusters of points in Fig. 1a (*E* region and *F* region) imply that the coherent echoes at a fixed group range can result in a superposition of backscatter with satisfactory orthogonality conditions from up to four ionospheric heights (e.g., intersections of the yellow and red contours along the gate 15 line). The relative contribution of the scatter from various heights to the resultant echo power detected by a radar depends on multiple factors, with the background electron density being among the most important ones (Uspensky et al., 1994). Accordingly, the velocity of received echoes would depend on the signal contributions from various heights.

To better estimate the echo power distribution in the lower ionosphere, and thus the most likely velocity of echoes, we performed ~50 tracings for each initial elevation angle at the radar. We then computed the averaged power of an echo at each location along the trajectory by assuming that it is proportional to the square of the local electron density (at the locations with the aspect angle being within $\pm 0.1°$) and inversely proportional to the cube of the range, similar to Uspensky et al. (1993; 2001).

Figures 1b,c show the height-range gate distribution of the expected echo power (in arbitrary units expressed in dBs), owing purely to propagation conditions, for the heights of 50-150 km. In Figure 1b, one can notice a steady decrease in the height of the strongest echoes at farther ranges for the pixels at the bottom side. This feature is less obvious in Fig. 1c. Also recognizable is the trend in the power-weighed height of echoes shown by crosses at each range gate. Constant height at increasing ranges would translate to a decrease in elevation angle. The tendency for the elevation angle to decrease with a range at short-range gates of 0-10 can be used as an additional identifying factor for SuperDARN echoes coming from the electrojet heights. At far ranges, the heights of strongest echoes are around the upper boundary of the electrojet layer for both 10 and 12 MHz, Figs. 1b,c.

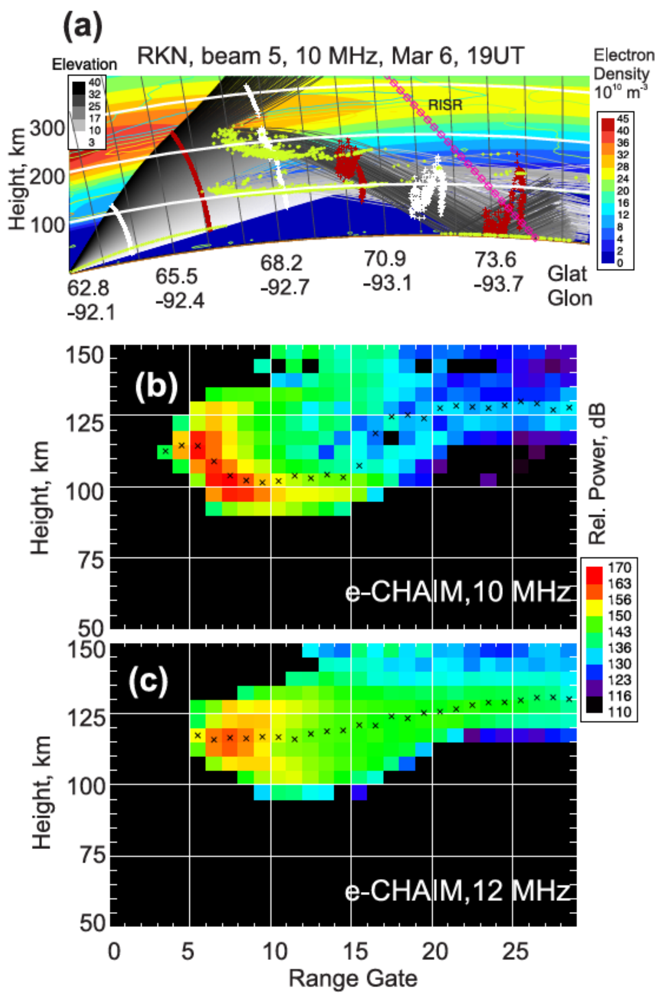

Figure 1: (a) Ray tracing for the 10 MHz radio waves transmitted at the location of the Rankin Inlet (RKN) radar along its beam 5 direction. The 2-D electron density distribution is given by the E-CHAIM electron density model (Themens et al., 2017) for 19 UT on 6 March 2016. White and red markers correspond to group range gates 0, 10, 20 and 5, 15, 25, respectively. Yellow markers are locations where radio waves are within $\pm 0.1°$ of the orthogonality with the Earth's magnetic field lines. (b) Expected power of 10 MHz echoes from various heights (between 50 and 150 km) as a function of RKN range gate. Arbitrary units were used (c) The same as (b) but for the radar frequency of 12 MHz. The sloped pink line in Fig. 1a represents those locations where the ISR at Resolute Bay measured the plasma flow velocity and electron density. These data will be discussed later.

At small range gates in a range profile of HF echo bands, the echoes are expected to come from two slightly different height regions within the electrojet layer. For a case of pure electrojet-related echoes (e.g., no irregularities present above the electrojet heights), the echo power would be stronger near the front edge of the *E* region points, as shown in Figs. 1b,c while at farther ranges the effective height of the backscatter decreases, and HF echoes are expected to come mostly from the bottom of the E region (Uspensky et al., 2001, their Figure 6). For a uniform distribution of the electric field in the ionosphere (at every height), it is expected that the Doppler velocity of E region echoes would decrease with range, being smallest at the far edge of the echo band (Uspensky et al., 2001). This feature, however, is not easy to recognize in SuperDARN data because of typically occurring latitudinal variations of the plasma drift velocity. In a case where an HF radar detects primary electrojet irregularities with a velocity close to the ion-acoustic speed C_S, the measured velocity should also decrease with range because of the scatter height decrease. An important conclusion from Figs. 1b,c is that 12 MHz echoes are expected to come from somewhat larger heights than 10 MHz echoes. This implies that the velocity of 10 MHz echoes is expected to be slightly smaller than that at 12 MHz if pure E region (electrojet) echoes are involved.

At somewhat farther range gates (>10, Figs. 1b,c), some echo power can come from above the electrojet heights, i.e. above 120 km. Such a situation has been expected for SuperDARN observations at range gates 10-20, ranges 700-1000 km (e.g., Danskin, 2003). Because the irregularities at these heights move with the $\mathbf{E}\times\mathbf{B}$ drift of the bulk plasma, the measured velocity should be close to the $\mathbf{E}\times\mathbf{B}$ drift component. Another expectation is that the Doppler spectrum of the echoes would contain multiple peaks (Danskin, 2003). The standard SuperDARN technique is not designed to handle multi-peak echoes; usually, only one of the velocity spectral peaks is identified (Danskin, 2003).

At far ranges of >1000 km (gates >20), the echoes are expected to come mostly from above the electrojet heights at F region heights, Fig. 1a. Although such echoes might come from many heights simultaneously, their velocity is the $\mathbf{E}\times\mathbf{B}$ component of plasma flow, i.e. about the same provided that the flow is uniform. We comment that the observed velocity at these ranges is actually smaller than the velocity of the bulk of plasma by the amount of the index of refraction: $V_{SuperDARN} = V_{irr} \cdot n$. This is because SuperDARN measurements assume that the radio waves scattering occurs in the vacuum while in reality it occurs in plasma with non-zero electron density. A number of SuperDARN studies (e.g., Gillies et al., 2009; Ponomarenko et al., 2009) concluded that the velocity of SuperDARN echoes received from the F region is reduced, up to 20%. Since the electron density in the regular E region is smaller than that in the F region, this “instrumental” effect is expected to be negligible for the E region echoes.

According to Figs. 1b,c there is a difference in the shortest ranges of echo detection, by 3-4 range gates. We note that depending on the vertical (and to some degree horizontal) distribution of the electron density, the relative location of the shortest ranges of echo detection varies so that they can be very close to each other and at very short ranges.

To investigate to what extent the above expectations for the velocity of HF echoes are correct we consider in this study observations by the Rankin Inlet (RKN) SuperDARN radar. This radar was selected because its beam 5 is directed toward Resolute Bay where ionospheric plasma parameters are measured with the incoherent scatter radar (see next section and Gillies et al. (2018)). Also, the RKN radar has elevation angle data of reasonable quality.

We consider in this study two approaches: one is to compare the RKN radar velocity data with $\mathbf{E}\times\mathbf{B}$ drifts measured by the ISR concurrently and the second one is to compare RKN velocity measurements at 10 MHz and 12 MHz. The idea behind the second approach is that, for two-frequency SuperDARN observations, echoes at the same range can come from the electrojet heights at one frequency and the *F* region heights at the other one. This kind of data cannot resolve all the outstanding problems but can provide useful insights. We consider in this study only daytime conditions near the equinoctial time when the orthogonality condition is much easier to achieve in the polar cap ionosphere because of generally high electron densities.

3. Case study: 06 March 2016 event

We first introduce the geometry of the Rankin Inlet SuperDARN radar observations in the Canadian Arctic.

3.1 Geometry of Rankin Inlet observations and Resolute Bay location

Figure 2 shows the field of view (FoV) of the RKN radar, starting from range gate 5, and its beam 5 (dark-shaded beam) that is looking over Resolute Bay where the incoherent scatter radar RISR-C is located. The RISR-C radar works generally in multiple beams (Gillies et al., 2016; 2018). In this study we consider data from an 11-beam experiment in the so-called "world-day" mode run on 06 March 2016. 5-min LOS plasma velocity data were considered. Our prime interest is RISR-C data collected in beam 3 because this beam is oriented almost ideally along the RKN radar beam 5 so that the HF velocity can be directly compared with the RISR-C velocity after projecting it onto a plane perpendicular to the magnetic field lines. From Fig. 1a one can conclude that the RISR-C measurements extend up to RKN range gate 9.

We also considered 2-D vectors of the $\mathbf{E}\times\mathbf{B}$ plasma flow inferred from multiple RISR-C beams, according to the procedure by Heinselman & Nicolls (2008), Fig. 2b. The $\mathbf{E}\times\mathbf{B}$ vectors in RISR-C measurements are traditionally given with $0.25°$ steps of the geographic latitude.

This study focuses on 3 hours of joint RKN-RISR-C measurements between 18:00 UT and 21:00 UT on 6 March 2016, Fig. 2b. In terms of RISR-C data, this is a very special event. The most important item is that the velocity, for many 5-min intervals, showed smooth changes with range/latitude and the errors in velocity estimates were relatively small. Over the period of interest, there was some variability in vector orientations (within $\pm 30°$) depending on the latitude and time (Fig. 2b), but this is not very critical for this study as the vector data were only used to confirm that the RKN beam 5 was monitoring echoes roughly along the direction of the $\mathbf{E}\times\mathbf{B}$ plasma flow. For measurements at the height of 110 km, centers of RKN range gates 9, 14 and 19 correspond to geographic latitudes of $\sim 68°$, $\sim 70°$, and $\sim 72°$.

The errors in RISR-C measurements are of particular concern, particularly at the lowest accessible geographic latitudes corresponding to farthest radar ranges with signals at large heights being weak. The farthest RISR-C ranges are, however, vital for this study because one would expect *E* region RKN echoes (through the direct propagation mode) to occur at RKN range gates <10. We note that for other events that we investigated (on the order of 40), the errors in RISR-C LOS velocity measurements at these far ranges were large, sometimes reaching >100%. The second not less important feature for this event is that the $\mathbf{E}\times\mathbf{B}$ velocity magnitudes were large, up to 1 km/s, as can be seen in Fig. 2b. Under this condition, strong driving of *E* region electrojet irregularities is possible through the FB instability.

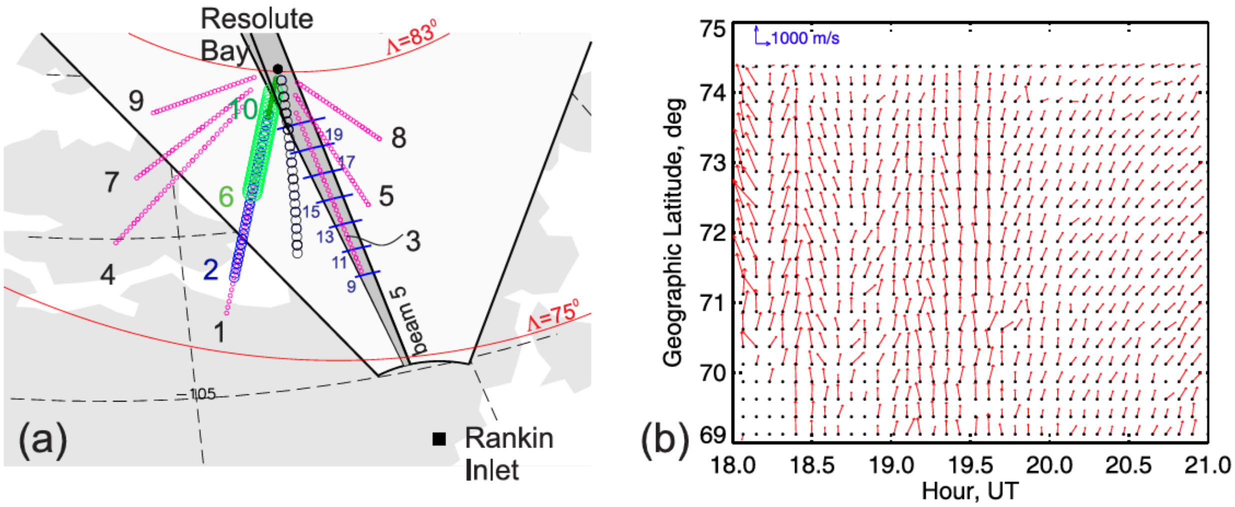

Figure 2: (a) Field of view (large white sector) of the SuperDARN radar at Rankin Inlet (RKN) for observations at 110 km and pierce points (at the height of 300 km) of the Resolute Bay (RB) incoherent radar RISR-C in the world-day experiment carried out on 6 March 2016 (colored circles). The darker narrow sector is the orientation of RKN beam 5, data from which (and adjacent beams 4 and 6) were considered. RISR-C radar beam 3 is oriented roughly along RKN beam 5. Black circles, stretching roughly along the magnetic meridian crossing the RB zenith, are locations vectors of the $\mathbf{E}\times\mathbf{B}$ plasma flow are provided, according to RISR-C measurements in multiple beams. The blue bars crossing beam 5 are centers of range gate 9, 11…21. The solid red arcs are lines of the geomagnetic latitude of $75°$ and $83°$. (b) Vectors of the $\mathbf{E}\times\mathbf{B}$ plasma flow inferred from RISR-C measurements on 06 March 2016 between 18:00 and 21:00 UT. Upward vector orientation implies flow exactly along the geographic North direction while orientation to the right means the eastward flow direction.

3.2 Rankin Inlet data

On 6 March 2016 the RKN radar, while operating with 1-min two-frequency switch mode, observed echoes for several hours in a row. Figures 3a-d show velocity and elevation data collected in beam 5 between 18:00 UT and 21:00 UT, separately for radar operating frequencies of ~10 and ~12 MHz. Importantly, at 19:00-20:00 UT, the echo band spanned from range gate 4 to range gates ~15-20 continuously, and echoes at farther ranges were also detected. Earlier in the event, the echo band was seen at range gates <20. These were determined to be *E* region echoes based on their elevation angle trends and low velocities. We note that the elevation angles in Figure 3 are the original ones but corrected by adding the instrumental phase delay of 3 ns, a typical value for the RKN measurements in 2016 (Ponomarenko et al., 2018).

In Figure 3 we mark, by a horizontal line on all panels, the location of range gate 10. This is a traditionally selected range gate delineating *E* and *F* region echo detection (e.g., Makarevich, 2010). 10 MHz elevation angle data of Fig. 3b show that this is indeed the range gate where a transition from *E* region to *F* region echo detection occurs. 12 MHz elevation angle data in Fig. 3d indicate that the *E* region echo detection extends to larger range gates ~15 at this frequency. The elevation angle values in Fig. 3 are consistent with expectations from the modeling, Fig. 1a.

One feature of short-range echoes in Figs. 3a-d is that the velocity magnitudes are comparable at two radar frequencies. The magnitudes are often larger than 300 m/s, especially at larger range gates of >20. An interesting feature is seen at ~18:30 UT. Here a clear band of high-velocity echoes (dark red blobs), limited in range, is seen in range gates 8-12 at 10 MHz, Fig. 3a. The 12-MHz band is also present, Fig. 3c, but it is shifted to larger range gates, as expected (Figs. 1b,c). The data collected in gates 8-10 thus indicate that the velocity of E region echoes at 10 MHz can be noticeably smaller than that at 12 MHz.

Between 18:00 and 19:00 UT, very low-velocity echoes of opposite polarity are seen in the lowest range gates, range gates 0-7. Morphologically, these short-range echoes can be classified as HAIR echoes (Milan et al., 2004) although one major difference with the previously discussed cases is that the echoes are very likely detected along the $\mathbf{E}\times\mathbf{B}$ flow direction. The flow direction was predominantly northward, according to RISR-C measurements, Fig. 2b.

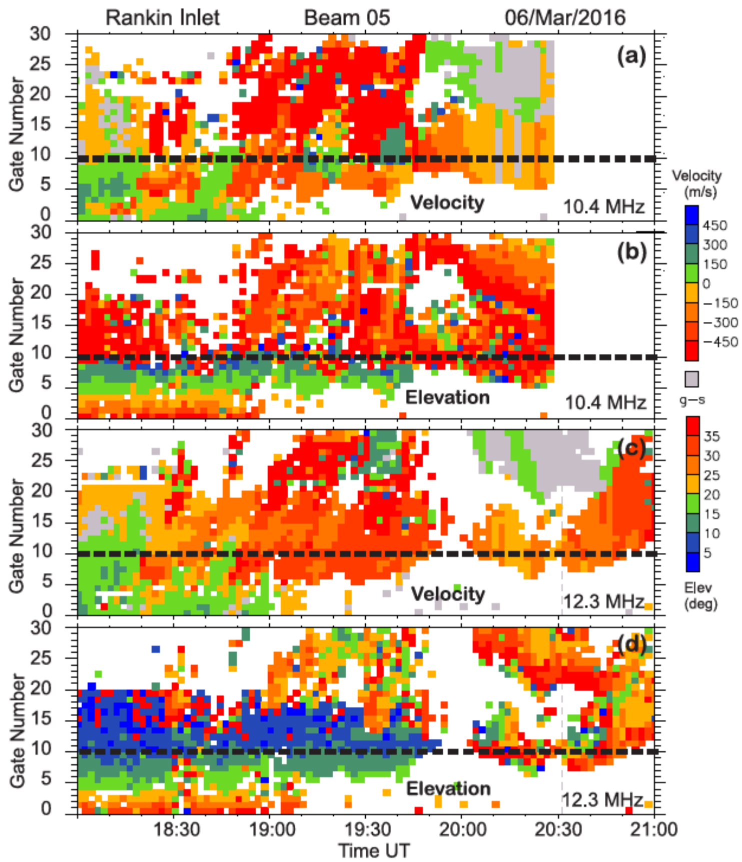

Figure 3: Rankin Inlet (RKN) radar data collected in range gates 0-30 of beam 5 for the event of 06 March 2016 (a) and (c) Doppler velocity at the radar operating frequency of ~10 MHz. and ~12 MHz, respectively. (b) and (d) Elevation angle of echo arrival for the radar operating frequency of ~10 MHz and 12 MHz, respectively. Range gate 10 is a traditionally accepted range gate boundary for a transition from the detection of E region echoes to F region echoes.

To establish a relationship between 10 MHz and 12 MHz RKN velocities in a more quantitative way, we performed a gate-by-gate comparison of velocities in several range gates for the period of 19:00-20:00 UT, Figs. 4a-f.

In range gate 6, the velocities are comparable in magnitude at two radar frequencies, Fig. 4a. The values are between 200 and 400 m/s with somewhat larger magnitudes at 12 MHz. In range gate 7, the 12 MHz velocity magnitudes are more obviously larger than those at 10 MHz. For data in gate 7, elevation angles (coded by color) are somewhat smaller. The effect of elevation angle decrease with range is expected if echoes are coming from the bottom part of the expected heights, Fig. 1a. We note that for both Fig. 4a and 4b, the velocity magnitudes reach 300-400 m/s, i.e. the nominal ion-acoustic speed C_S .

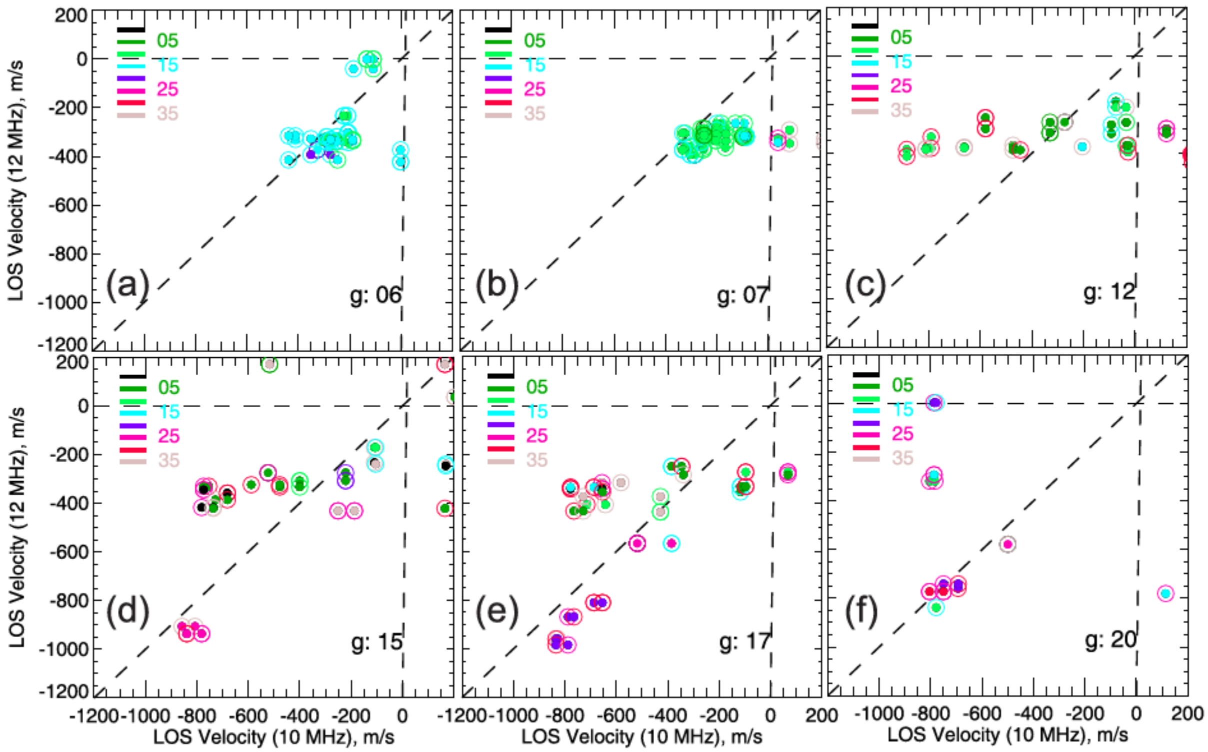

Figure 4: Scatter plots comparing RKN LOS velocities at 12 MHz and 10 MHz measured in the same range gates (these are shown in the right bottom corner of each plot) of beam 5 separated in time by not more than 1 min. The data are for 6 March 2016 between 19:00 UT and 20:00 UT. Each circle is colored according to the elevations angle with a scheme shown at the top left corner. The outside part of each circle reflects the elevation angle measured at 10 MHz while the inside solid dot reflects the elevation angle measured at 12 MHz. Gate number and the total number of points involved are given at the bottom.

Data in range gate 12 show quite a different pattern. Here 10 MHz velocities spread between -800 and 0 m/s while 12 MHz velocities are clustered along the line of -300 m/s. Elevation angle data indicate that, while 12 MHz echoes have about the same angles of arrival as in gates 6,7 (echoes from the *E* region heights, the green color of the circles center parts), the 10 MHz echoes have large elevation angles, see red outer parts of most of the circles. Thus, the 10 MHz echoes were received from above the electrojet heights. The significant differences in the echo velocity are then not a surprise.

Points with large differences between 10 and 12 MHz velocities are seen in range gates 15 and 17. These plots show one additional important feature, a set of points with the velocity magnitude of

~600-800 m/s at both 10 MHz and 12 MHz. The elevation angles for these points are high and comparable indicating that these echoes were received from *F* region heights. One subtle tendency here is that the 12 MHz velocity magnitudes are slightly larger than those at 10 MHz. This is expected for the SuperDARN *F* region echoes. Data in gate 20 show mostly large velocity magnitudes, comparable at the two radar frequencies. These are echoes from the *F* region heights.

One important conclusion from the data presented in Figure 4a-f is that at intermediate range gates, between ~11 and ~20, the 10 MHz and 12 MHz velocities can be quite different in magnitude. More typically the 12 MHz velocity magnitudes were smaller than the 10 MHz velocity magnitudes. For these cases, while 10 MHz echoes were received from the *F* region heights, 12 MHz echoes were coming from the electrojet heights.

3.3 Range **profiles for RKN velocity and $\mathbf{E}\times\mathbf{B}$ drift**

For comparison with RISR-C measurements we considered 5-min RISR-C plasma velocity data in beam 3. We note that Gillies et al. (2018) used 1 min data, but we found that their variability and errors in measurements are too high for the current comparison. Unfortunately, there were no good measurements of plasma temperature and electron density at the *E* region heights. The electron densities at the *F* region heights were of reasonable quality but these measurements are done near the Resolute Bay zenith, far away from most of the space where the RKN radar waves propagate, see Fig. 1a where we show the locations of RISR-C gates of measurements in its beam 3 at various heights with respect to RKN. Obviously, the RISR-C coverage of space needed for rays tracing analysis is not sufficient. This was the reason we used the E-CHAIM statistical model of the electron density distribution for ray tracing in Figs. 1a-c.

Figure 5 shows RKN LOS velocity data in various range gates of beam 5 over 19:00 - 19:12 UT and the RISR-C LOS velocity data in beam 3 (for the closest interval), projected onto the plane perpendicular to the magnetic field lines. The RISR-C velocities are given by black crosses with vertical black bars indicating the error of measurements (the ISR velocity polarity was changed to be consistent with the RKN direction of observations). The RKN LOS velocity values in Figs. 5a,b are color-coded according to the elevation angle measured. The velocity medians for each radar frequency (10 and 12 MHz) are presented in Fig. 5c along with the standard deviation of the velocity for each range gate of the observations shown by a vertical bar of an appropriate color. Standard deviations can be treated as a proxy for errors in RKN velocity measurements. We remind the reader that routine SuperDARN LOS velocities do not have errors computed; it is known, however, that they are typically on the order of 50 m/s (Ponomarenko, 2013; Reimer et al., 2018).

Figures 5a and 5b show that at very short ranges, the RKN velocities at two radar frequencies are small and comparable. This is not a surprise because the echoes at these ranges are very likely a scatter from irregularities produced by meteor-related processes and neutral wind turbulence at the bottom *E* region, heights of ~ 90-95 km (e.g., Yakymenko et al., 2015). Staring from range gate 5, *E* region/electrojet echoes are detected. Three aspects are worth mentioning. First, the elevation angles for these echoes decrease with a range as expected. Second, the *E* region echoes extend all the way to gate ~14 at 10 MHz and to gate ~17-18 at 12 MHz. Both values are well above the "nominal" value of 10. Finally, "typical" values of the velocity magnitude at 10 MHz are slightly smaller than those at 12 MHz. This feature is seen for the velocity medians shown in Fig. 5c and consistent with the data of Fig. 3. In Figure 5a and Fig. 5b, two horizontal lines of -400 m/s and -300 m/s indicate the range of nominal C_S values at the E region heights

Starting from range gate 15 at 10 MHz and 18 at 12 MHz, velocity magnitudes are much larger, above those observed around range gate 10 (by a factor of two). These echoes have large elevation angles. These are the scatter from F region irregularities, as expected, see the model predictions in Fig. 1a. RISR-C shows somewhat larger LOS velocity magnitudes, but the RKN velocities still can be judged as compatible with the $\mathbf{E}\times\mathbf{B}$ drift component if one takes into account the fact the HF velocity is reduced with respect to the plasma drift component due to "index of refraction effect" (Gillies et al., 2009; Ponomarenko et al., 2009). This effect can also explain the fact that the 12 MHz velocity magnitudes are slightly larger than those of the 10 MHz, the effect is clearly seen in Fig. 5c.

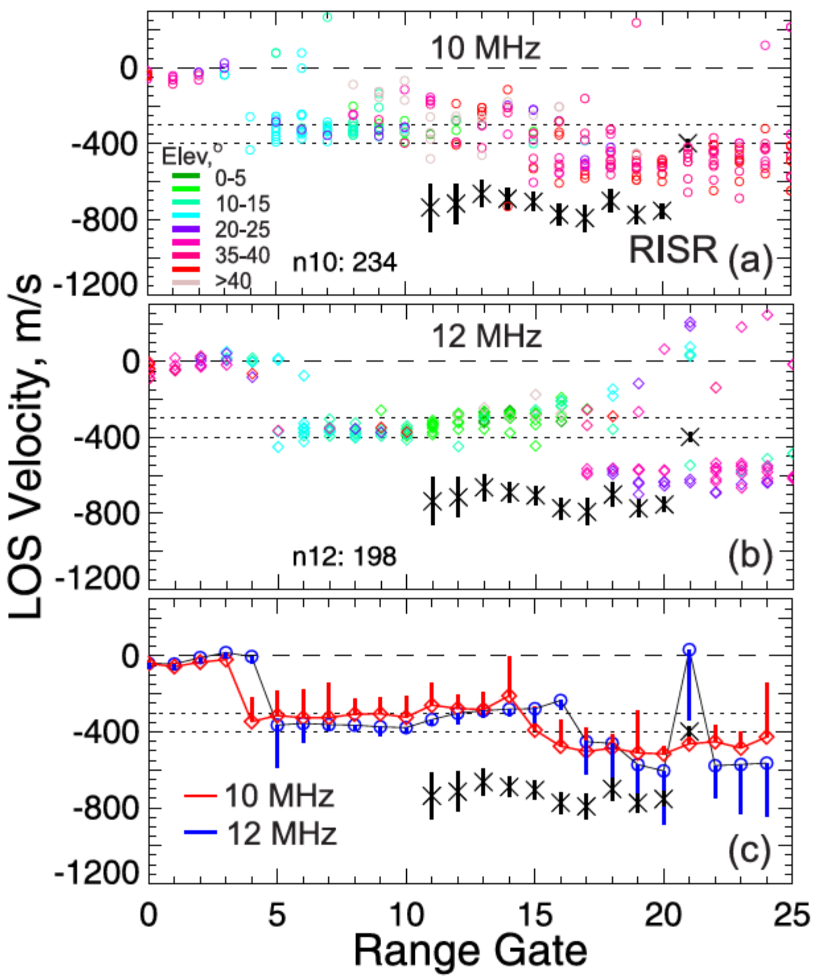

Figure 5: Scatter plots of RKN LOS velocity versus range gate for 10 min period of observation on 6 March 2016 between 19:00 and 19:10 UT. (a) and (b) are for 10 MHz and 12 MHz RKN transmissions, respectively. (c) Velocity medians in each range gate. The total number of points is shown at the bottom of each panel. Dashed lines indicate the range of nominal ion-acoustic velocity C_S at the electrojet heights.

3.4 RKN velocity and $\mathbf{E}\times\mathbf{B}$ drift for co-located points

Figure 5 indicates that the RKN velocity and the $\mathbf{E}\times\mathbf{B}$ drift component can be compared at close locations. The scattering regions monitored by the instruments are not quite coinciding but, considering the 45-km resolution of RKN measurements, spatial differences by 50 km can be considered as tolerable. In addition, the latitudinal (range) variations of the RISR-C velocity were not strong most of the time for the event under consideration (this was one of the reasons for this event selection). We also decided to consider RKN data in three beams, 4-6, to increase the data statistics, and this smoothed the actual RKN velocity values.

Figure 6 is a scatter plot of the RKN velocity (5-min medians over beams 4-6) versus the $\mathbf{E}\times\mathbf{B}$ velocity component measured by RISR-C radar in beam 3 and projected onto a plane perpendicular to the magnetic field lines. Data for the RKN 10 MHz and 12 MHz operating frequencies are shown by red and blue circles, respectively.

One obvious and highly expected feature of Fig. 6 is that the vast majority of points are located between the zero RKN velocity line and the bisector of perfect agreement between the instruments. The 12 MHz data show a clearer pattern. One feature is that the cloud of blue points, between -200 and -400 m/s, is stretched "horizontally" from -400 m/s to -1000 m/s of the $\mathbf{E}\times\mathbf{B}$ component. These are cases of *E* region echo detection at 12 MHz. The velocity magnitudes are below 400 m/s. The black line in Fig. 6 is the dependence of C_S upon $\mathbf{E}\times\mathbf{B}$ magnitude as reported by Gorin et al. (2012) for the height of 102 km. At larger heights, the expected dependence is much stronger. One can say that the 12 MHz data show values below the expected values and there is no expected increase of the RKN velocity at the largest $\mathbf{E}\times\mathbf{B}$ drifts. There are not too many of this type of points for the 10 MHz data with typical velocity magnitudes being below 200 m/s.

Another cloud of points is for $\mathbf{E}\times\mathbf{B}$ drifts between -1100 and -700 m/s. Here both red and blue circles are clustered close the bisector of perfect agreement, with the red circles departing somewhat more from the bisector. These points correspond to the detection of the *F* region echoes at both RKN frequencies.

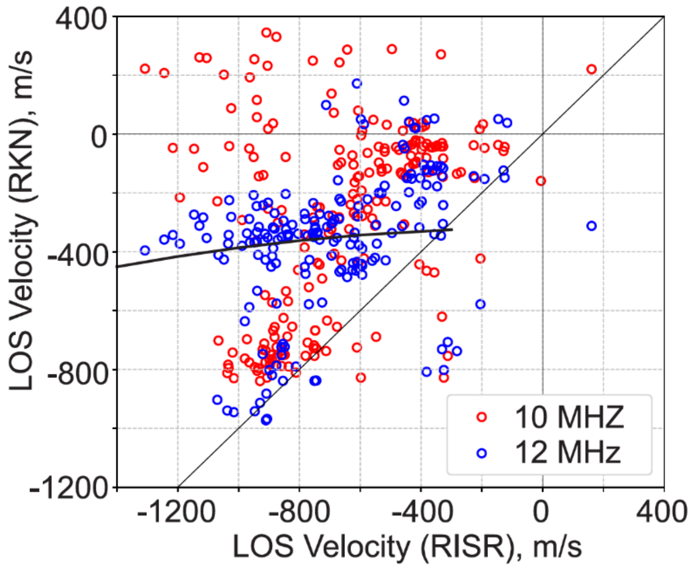

Figure 6: Scatter plot of the RKN LOS velocity medians observed in beams 4-6 versus the $\mathbf{E}\times\mathbf{B}$ velocity component along beam 3 projected onto a plane perpendicular to the magnetic field lines. Matched in time (5-min periods of RISR-C measurements) and co-located (in range) measurements were considered. Data for 10 and 12 MHz RKN operating frequency are shown by red and blue circles, respectively.

Finally, one can recognize in Fig. 6 a cluster of low-velocity data at both frequencies, with magnitudes below 100-150 m/s. Such echoes exist even for large $\mathbf{E}\times\mathbf{B}$ drifts of ~ 1000 m/s. We note that VHF radars would normally detect high-velocity echoes for such fast plasma flows (Nielsen & Schlegel, 1985). This points at the non $\mathbf{E}\times\mathbf{B}$ related source of ionospheric irregularities responsible for low-velocity echoes.

4. Velocity of HF echoes in the transition region, analysis for a larger database

The data presented indicate the occurrence of events with echo detection from the electrojet heights at 12 MHz and from the *F* region heights at 12 MHz. To show that these are not so rare-occurring events for the daytime RKN observations we consider here an extended database. To create it, we searched through March and April of 2016 and 2012 RKN observations and selected all the events with latitude-extended echo bands, both in time and range, so that the echoes from the transition region between *E* region and *F* region echo detection were available. The list of the selected events is given in Table 1.

Table 1. List of events selected for the analysis

Year	Month	Day	UT start	UT end
2016	March	6, 8,9,10,11,12,18,19,20,22,23,28,29,30	14	21
2016	April	2,3,5,6,7,23,27	14	21
2012	March	17,19,21,22,24,27,31	14	21
2012	April	1,2,5,10,14,21,23,24,25,28,29	14	21

To further increase statistics, data in two RKN beams 5 and 6 were considered. Several sets of range gates were chosen, at typical ranges of pure *E* region echo detection (range gates 5-7), at ranges of pure *F* region echo detection (range gates 20-22) and in the transition region between the two (range gates 11-16). For each set of ranges and two radar beams, velocity medians were computed, separately for 10 MHz and 12 MHz measurements, and then matched in time (with 10 and 12 MHz measurements being separated by less than 2 min). Velocity medians were then entered into a common database.

Figure 7 presents velocity medians, binned further for presentation in two formats: the straight point-by-point velocity comparison, panels (a)-(c), and as the velocity ratio $R_1 = Vel_{12\,\mathrm{MHz}} / Vel_{10\,\mathrm{MHz}}$ as a function of LOS velocity measured at 10 MHz, panels (d)-(f). For the first comparison, 50×50 m/s velocity bins were adopted. For the second comparison, bins for the velocity were the same while bins for the ratio R_1 were selected between -1 and 3 with a step of 0.1.

Data in typical ranges of pure *E* region echo detection (range gates 5-7), Figs. 7a,d, show that the velocities are close to one another. Points are scattered but the majority are located close to the bisector of perfect agreement in Fig. 7a or R_1 being close to 1, Fig. 7d. The ratio R_1 is also close to 1 at typical ranges of pure *F* region echo detection, gates 20-22, Fig. 7f. Data for intermediate-range gates 11-16, Fig. 7b,e, clearly shows the occurrence of two separate clouds of points. Many points are scattered along the bisector of perfect agreement. These are the expected cases of *F* region echo detection at both radar frequencies. Fewer points, but still noticeable, form a cloud that is stretched "horizontally" at relatively small 12 MHz velocity magnitudes of 0-300 m/s for 10 MHz velocities in between zero and -800 m/s of. The occurrence of the two separate clusters is more evident in the 2-D distribution of Fig. 7e for R_1; one maximum (red pixels) with R_1~1 is at velocities of ~270-300 m/s and the second maximum with R_1~0.2 is at velocities of ~ -350 m/s.

Figure 7 data are consistent with the major features identified for the 6 March 2016 event. They support the notion that events with 12 MHz echoes having velocity magnitudes much smaller than those of 10 MHz echoes are not a rare occurrence.

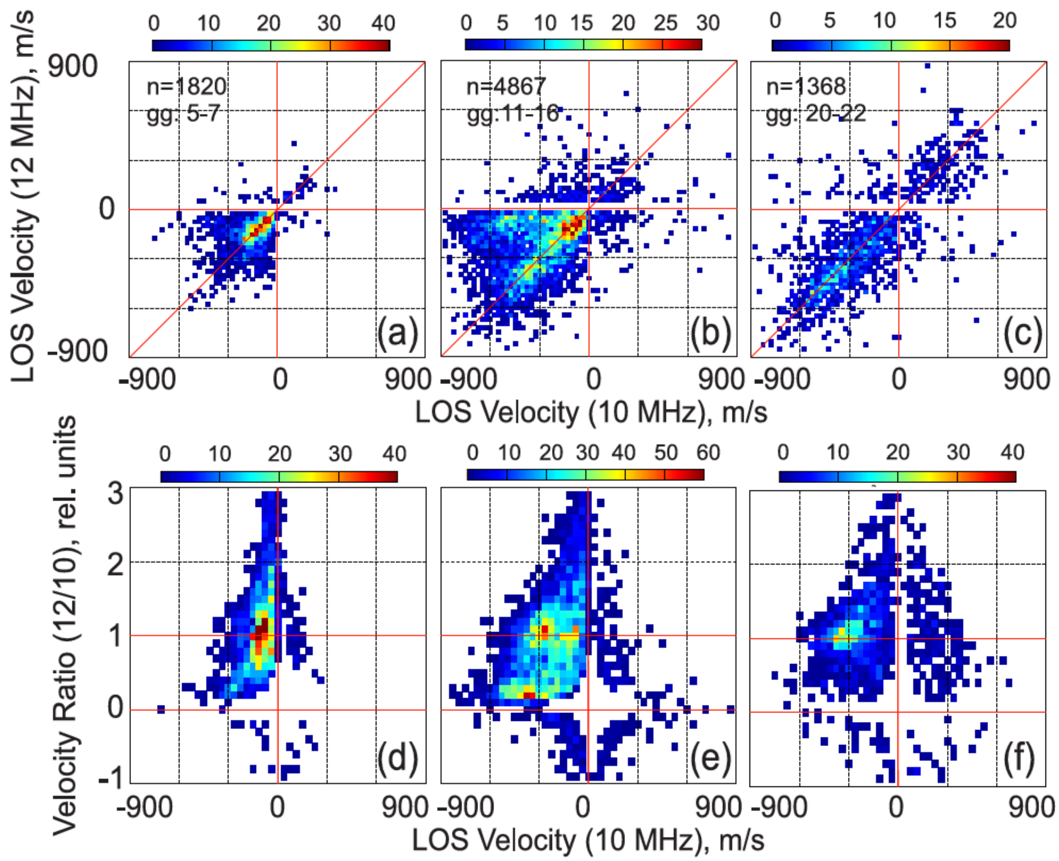

Figure 7: (a) – (c) Scatter plots of RKN velocity at 12 MHz versus RKN velocity at 10 MHz. The color reflects the number of points in each pixel of the velocity. Panels (a), (b) and (c) are for a set of range gates as reported at the top of each panel. The total number of points available is also shown. (d) – (f) Scatter plots of velocity ratio $R_1 = Vel_{12\,\mathrm{MHz}} / Vel_{10\,\mathrm{MHz}}$ for the same sets of gates as for (a)-(c).

The frequent occurrence of relatively low 12-MHz velocities in range gates 10-20 is somewhat unexpected on the basis of a simple overview of SuperDARN radar range-time plots for the velocity or elevation angle. One might think that the above results are a consequence of a special selection of the events undertaken above. To investigate how significant the effect is overall we considered all RKN daytime (16-21 UT) observations in the dual 10/12 MHz mode over four months around equinoctial time as a representative period of SuperDARN measurements (March, August, September, and October of 2016). We further limited the database to those cases when the velocity of 10 MHz echoes was above 300 m/s. In these cases, the measured velocity might well be representing the fast $\mathbf{E} \times \mathbf{B}$ plasma flow (F region scatter) albeit not all the time because on some occasions it could be representing detection of E region echoes. If in these cases 12 MHz echoes were received from the electrojet heights, their velocity is expected to be close to or below C_S so that the velocity ratio $R_2 = Vel_{10\,\mathrm{MHz}} / Vel_{12\,\mathrm{MHz}}$ would be larger than 1.5-2. Our goal was to assess the R_2 values for the data set selected statistically.

Figure 8 shows histogram distributions of R_2 values for four bands of range gates, typical E region echo detection (range gates 5-10), two intermediate ranges (11-16 and 17-22) and typical pure F region echo detection gates (23-25). For the histogram distributions of Fig. 8, we computed percentages of cases with R_2 values being between 2 and 4, out of all cases in each band of ranges. We assume that the R_2 values between 2 and 4 can be, at least partially, associated with E region echo detection at 12 MHz and F region echo detection at 10 MHz.

Figure 8a shows that at traditional range gates of E region echo detection (5-10), there are about 25% of cases with significantly larger 10 MHz velocities as compared to those at 12 MHz. This number is also 25% when considering gates 11-16 (Fig. 8b), and it is much smaller for range gates 17-22 (Figs. 7c, 10%) and 23-25 (Fig.8d, 7%), as expected, on the basis of the previous analysis.

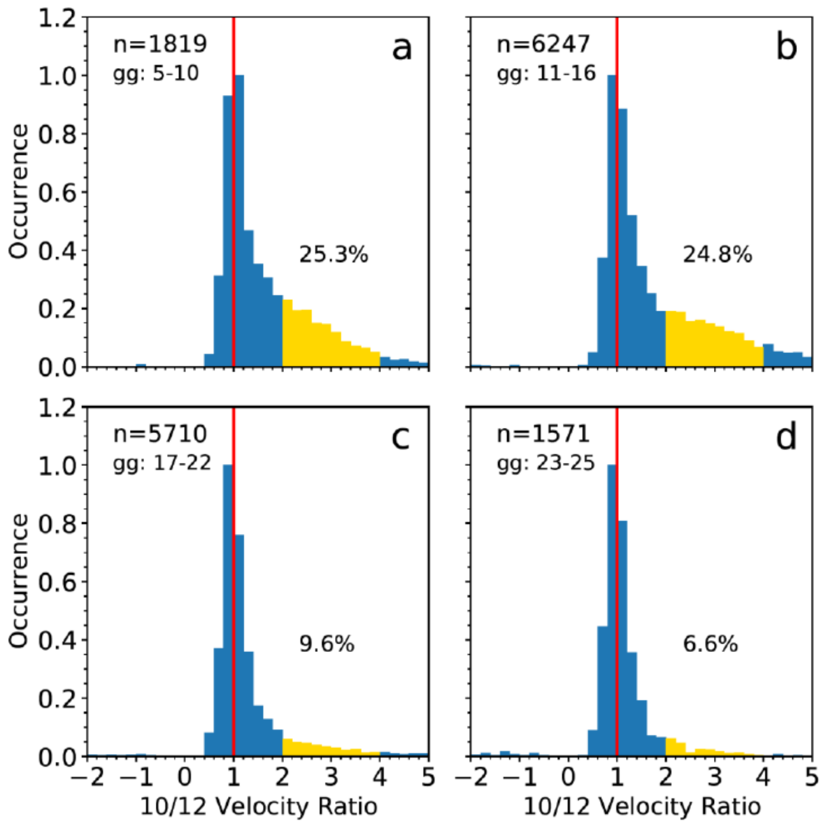

Figure 8: Histogram distribution of the RKN velocity ratio $R_2 = Vel_{10\mathrm{MHz}} / Vel_{12\mathrm{MHz}}$ during daytime (16-21 UT) for observations in March, August, September and October of 2016. Only cases with the 10-MHz RKN velocity magnitude above 300 m/s were considered. Each plot is for a band of radar range gates shown in the top-left corner. Also shown in the top-left corner is the total number of measurements available. The vertical red line is the ideal case of the ratio being 1. Also presented is the percentage of cases where R_2 is between 2 and 4.

5. Discussion

A possibility of simultaneous HF echo reception from the electrojet heights and well above it, including from the heights of the *F* region electron density peak, has been anticipated since the beginning of the SuperDARN operation in 1990s. The relationship of the SuperDARN velocity and the $\mathbf{E}\times\mathbf{B}$ drift at these ranges has, nevertheless, been investigated poorly. The most valuable contribution comes from a recent study by Gillies et al. (2018) who compared RKN velocities and $\mathbf{E}\times\mathbf{B}$ drift measured by RISR-C radar at RKN range gates 10-20. The major result reported is that SuperDARN velocities are smaller than the $\mathbf{E}\times\mathbf{B}$ drift by a factor of 2 for daytime observations and close to, or even lager than, the $\mathbf{E}\times\mathbf{B}$ drift for nighttime observations, their Fig. 4.

Gillies et al. (2018) performed a refined analysis for nighttime measurements where the authors focused on measurements in gates 10-14 thinking that at these range gates the RKN radar detects signals only from the electrojet heights. The RKN velocities were found to be comparable with LOS $\mathbf{E}\times\mathbf{B}$ drifts whenever the drift was around 300-500 m/s. For faster flows, RKN velocities were well below the $\mathbf{E}\times\mathbf{B}$ LOS component. However, for slower drifts, RKN velocities were found to be well above the LOS $\mathbf{E}\times\mathbf{B}$ component. The authors argued that this result is probably an artifact of observations under strongly variable $\mathbf{E}\times\mathbf{B}$ nighttime flows and associated large error bars in measurements. This was certainly the case for 1min data used by Gillies et al. (2018), and for this reason, in this study we considered 5-min averaged RISR-C data and selected a single event with relatively smooth spatial and slow temporal variations of the $\mathbf{E}\times\mathbf{B}$ drift.

For the daytime observations, Gillies et al. (2018) reported that the RKN velocity was statistically smaller than the $\mathbf{E}\times\mathbf{B}$ drift LOS component by a factor of ~2, their Fig. 4. This is consistent with what we report in this study for the 6 March 2016 event, Fig. 6, which was a part of the database analyzed by Gillies et al. (2018). We found here that the effect seems to be stronger for 10 MHz transmissions, our Fig. 6.

Our analysis of the 6 March 2016 event showed that the *E* region echoes ranges can be well beyond the gate 10 and even gate 14, reaching gates 16-17 for the 12 MHz operating frequency, our Fig. 5. In the past, the focus was on high-velocity *E* region echoes detected with 1&1/2-hop signal propagation mode, at range gates ~40 (e.g., Gillies et al., 2018). In the present study, we considered short ranges with echo detection through the direct mode.

We note that in agreement with previous studies we showed that the velocity of *E* region HF echoes is close to the nominal speed of ion-acoustic waves of C_S =350-400 m/s traditionally cited in the past. One distinct feature identified (Figure 6) is that the 12 MHz velocities were about the same, independent of the $\mathbf{E}\times\mathbf{B}$ magnitude up to ~1000 m/s. This is somewhat unexpected because the ion-acoustic speed at high latitudes should increase with the $\mathbf{E}\times\mathbf{B}$ magnitude increase. We showed in Fig. 6 the expected trends for the height of 102 km. A stronger curving of the dependence is expected at larger heights (Gorin et al., 2012), and the HF data of Fig. 6 are inconsistent with those. The relatively small values of HF velocity reported in the present study can be interpreted in terms of HF echoes detection from the electrojet bottom side. Gorin et al. (2012) argued that this is a typical situation for the auroral oval ionosphere where electron densities are high enough to bend HF radio waves to achieve the orthogonality at low heights. Interestingly, statistical analysis of SuperDARN data showed that typical velocities of short-range echoes are close or below the nominal C_S value as well (Makarevich, 2008; 2010).

Another subtle effect for the *E* region data presented in Figs. 4-6 is that the 10 MHz velocities are statistically slightly smaller than the 12 MHz velocities. This is very likely due to the fact that 12 MHz echoes are expected to come from slightly larger heights with a slightly larger velocity of electrojet irregularities, see Figs. 1b,c. Thus, contrary to the case of *F* region echoes, gate-by-gate comparison of *E* region HF velocities may not reflect the physics of electrojet irregularities as considered in the past (i.e., Hanuise et al., 1992).

Data presented in this study give additional information on a possible range extent of *E* region echoes. Figures 3-5 indicate the occurrence of *E* region echoes all the way to range gates ~20 at 12 Hz. Our review of RKN data for March and April 2012 and 2016 showed that this is an unusually large number for daytime observations. Typically, the boundary is located at gate ~15 for 12 MHz and at gate ~10 for 10 MHz. In addition, our analysis showed that the occurrence of *E* region echoes with much smaller 12 MHz velocities as compared to those at 10 MHz (and presumably, $\mathbf{E}\times\mathbf{B}$ drift component), within the transition region is not so rare a phenomenon for the RKN radar, comprising up to 25% of daytime high-velocity cases.

The occurrence of low-velocity echoes, sometimes at both typical radar frequencies, can lead to some changes in the shape of SuperDARN convection patterns (Chisham and Pinnock, 2002) and the underestimation of the cross polar cap potential (CPCP) inferred from the SuperDARN convection maps. Investigation of these changes is beyond the scope of this study. Here we focus on one aspect, namely the effect of including SuperDARN velocities at all ranges in the processing of convection maps. We note that although Thomas and Shepherd (2018), while producing their statistical model of SuperDARN patterns, removed all radar data from range gates below 14 and above 45, it is not known to what the extent this restriction has been and is currently applied to actual SuperDARN data processing in various studies.

Figure 9 shows two SuperDARN convection maps processed first by including all radar network data at all ranges (case (a), Fig. 9a) and by excluding all network radar data at range gates below 14 and above 45, as adopted by Thomas and Shepherd (2018), case (b), Fig. 9b. In Figure 9c we compare the CPCP values for the 2-min maps processes in these two ways for the period of 18:00-21:00 UT on 6 March 2016.

One can notice slightly fewer points in Fig. 9b. The convection patterns in Fig. 9a and Fig. 9b are about the same in their shape. One can visually notice that the dawnside flows are slower for the case (a) in the polar cap and at the auroral zone latitudes. The CPCP is smaller for the case (a) by 7 kV for this specific moment. A scatter plot in Fig. 9c shows that smaller CPCPs for case (b) hold for the majority of points. The median of the differences is 4 kV.

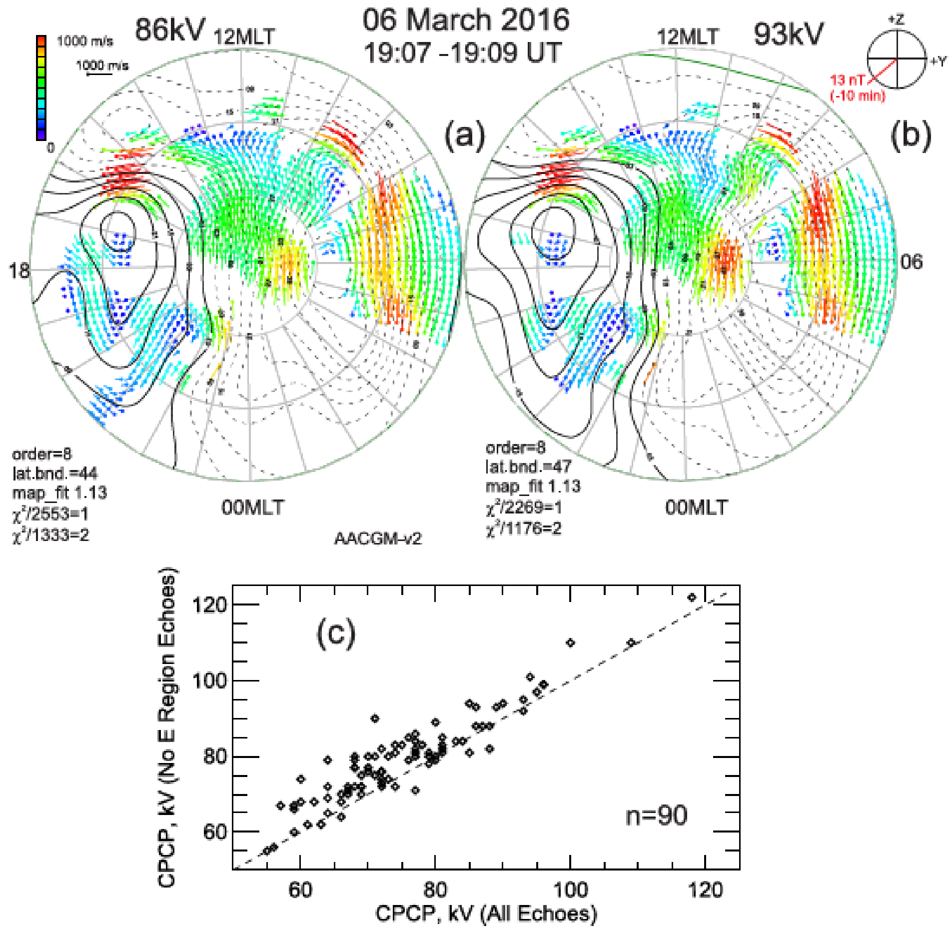

Figure 9: (a) and (b) SuperDARN convection maps built for 19:07-19:09 UT on 6 march 2016 with the application of the statistical convection model by Thomas and Shepherd (2018) and considering data from all the SuperDARN radars. (a) Radar velocity data in all range gates considered. (b) Radar velocity data only in ranges gates 15-45 considered. (c) Inferred cross polar cap potential (CPCP) for case (b) versus the CPCP for case (a) for the period of 18:00 - 21:00 UT.

6. Summary and conclusions

In this study, we investigated to what extent the velocity of SuperDARN RKN radar echoes at intermediate ranges (gates 10-20) is related to the $\mathbf{E}\times\mathbf{B}$ drift of the plasma by employing direct comparison with drift measurements by the ISR in the co-located beams and by comparing HF velocities at two RKN radar frequencies, 10 and 12 MHz.

We identified one event with echo bands extending from small range gates of ~4 to large range gates of >25 to show that the velocities at 10 MHz at intermediate ranges are often larger than the velocity at 12 MHz by 2 and more times. Concurrent $\mathbf{E}\times\mathbf{B}$ drift measurements by the ISR indicated that the velocity of 10 MHz echoes was smaller, but not dramatically, than the $\mathbf{E}\times\mathbf{B}$ LOS component along the radar beams. In this case, the large differences between 10 MHz and 12 MHz velocities were clearly because 12 MHz echoes were received from the electrojet heights while the 10 MHz were received from the F region heights. RKN elevation angle data were shown to be consistent with this interpretation.

The 12 MHz E region echo detection was possible all the way to range gate 17-18. At larger range gates, the radar was receiving echoes from the F region with velocities smaller than, but close to the $\mathbf{E}\times\mathbf{B}$ drift. A similar pattern of velocity changes was found for observations at 10 MHz, but the transition region occurred at smaller range gates of ~11.

By looking at a number of similar events, spread over 4 different months of RKN observations, we showed that the situation with low 12 MHz velocities and high 10 MHz velocities is fairly frequent. Finally, by considering all the short-range echo events over four different months, without requiring echo presence in a wide range of gates, we estimated that for large velocities at 10 MHz (above 300 m/s), the velocity of 10 MHz echoes was larger than the velocity of 12 MHz echoes (by a factor of 2-4) in ~10-20% of cases, depending on range gates selected. The analysis performed implies that the transition boundary from E to F region echo detection varies with propagation conditions and is very unsettled.

A large number of echoes with velocities close to the ion-acoustic speed C_S were observed, predominantly in range gates 5-16. Such echoes were detected at closer range gates at 10 MHz as compared to those at 12 MHz, but the echoes at both radar frequencies co-existed in many range gates. The echo velocity magnitudes were <350-400 m/s most of the time, i.e. below the expected nominal ion-acoustic speed of >400 m/s and the expected effect of the velocity increase as a function of $\mathbf{E}\times\mathbf{B}$ magnitude was not found.

Finally, we assessed the potential effect of low-velocity E region data inclusion in the process of SuperDARN convection maps construction. For a 3-hour event with large flow velocities we showed that the shape of the pattern does not change dramatically but the cross polar cap potential is reduced by several kilovolts.

Acknowledgments

The SuperDARN data used in this work were collected with the support of the Canadian Space Agency's Geospace Observatory (GO Canada) continuation initiative, the Canada Foundation for Innovation, and the Province of Saskatchewan. SuperDARN data can be obtained from https://superdarn.ca. The University of Calgary RISR-C radar is funded by the Canada Foundation for Innovation and is a partnership with the US National Science Foundation and SRI International who also fund RISR-C radar operation. RISR-C data are available at http://data.phys.ucalgary.ca/. The research was supported by an NSERC Discovery grant to A.V.K.

References

Bahcivan, H., Hysell, D. L., Larsen, M. F., & Pfaff, R. F. (2005). The 30-MHz imaging radar observations of auroral irregularities during the JOULE campaign. *Journal of Geophysical Research: Space Physics, 110*, A05307. https://doi.org/10.1029/2004/JA010975.

Chisham, G., & Pinnock, M. (2002). Assessing the contamination of SuperDARN global convection maps by non-*F*-region backscatter. *Annales Geophysicae, 20,* 13 – 28. https://doi.org/10.5194/angeo-20-13-2002.

Chisham, G., Lester, M., Milan, S. E., Freeman, M. P., Bristow, W. A., Grocott, A., McWilliams, K. A., Ruohoniemi, J. M., Yeoman, T. K., Dyson, P., Greenwald, R. A., Kikuchi, T., Pinnock, M., Rash, J., Sato, N., Sofko, G., Villain, J.-P., & Walker, A. D. M. (2007). A decade of the Super Dual Auroral Radar Network (SuperDARN): Scientific achievements, new techniques and future directions. *Surveys of Geophysics, 28*, 33–109. https://doi.org/10.1007/s10712-007-9017-8.

Danskin, D. (2003) HF auroral backscatter from the *E* and *F* regions. PhD Thesis, U of Saskatchewan, Saskatoon, Canada. https://harvest.usask.ca/handle/10388/etd-10242003-121305.

Dimant, Y. S., & Sudan, R. N. (1995). Kinetic theory of the Farley- Buneman instability in the *E*-region of the ionosphere. *Journal of Geophysical Research: Space Physics, 100,* 14605–14623. https://doi.org/10.1029/95JA00794.

Dimant, Y. S., & Sudan, R. N. (1997). Physical nature of a new cross-field current-driven instability in the lower ionosphere. *Journal of Geophysical Research: Space Physics, 102*, 2551–2563. https://doi.org/10.1029/96JA03274.

Fejer, B. G., & Kelley, M. C. (1980). Ionospheric irregularities. *Reviews of Geophysics, 18*, 401–454. https://doi.org/10.1029/RG018i002p00401.

Gillies, R. G., Hussey, G. C., Sofko, G. J., McWilliams, K. A., Fiori, R. A. D., Ponomarenko, P., & St. Maurice, J.-P. (2009). Improvement of SuperDARN velocity measurements by estimating the index of refraction in the scattering region using interferometry. *Geophysical Research Letters, 114*, A07305. https://doi.org/10.1029/2008JA013967.

Gillies, R. G., van Eyken, A., Spanswick, E., Nicolls, M. J., Kelly, J., Greffen, M., et al. (2016). First observations from the RISR-C incoherent scatter radar. *Radio Science, 51*, 1645-1659. https://doi.org/10.1002/2016RS006062.

Gillies, R. G., Perry, G. V., Koustov, A. V., Varney, R. H., Reimer, A. S., Spanswick, E., St.-Maurice, J.-P., & Donovan, E. (2018). Large-scale comparison of polar cap ionospheric velocities measured by RISR-C, RISR-N, and SuperDARN. *Radio Science, 53*. https://doi.org/10.1029/2017RS006435.

Gorin, J. D., Koustov, A. V., Makarevich, R. A., St-Maurice, J.-P., & Nozawa, S. (2012). Velocity of *E*-region HF echoes under strongly-driven electrojet conditions. *Annales Geophysicae, 30*, 235–250. https://doi.org/10.5194/angeo-30-235-2012.

Greenwald, R. A., Baker, K. B., Dudeney, J. R., Pinnock, M., Jones, T. B., Thomas, E. C., Villain, J.-P., Cerisier, J.-C., Senior, C., Hanuise, C., Hunsuker, R. D., Sofko, J. G., Koehler, J. A., Nielsen, E., Pellinen, R., Walker, A. D. M., Sato, N., & Yamagishi, H. (1995). DARN/SuperDARN: A global view of the dynamics of high-latitude convection. *Space Science Reviews, 71*, 761-796. https://doi.org/ 10.1007/BF00751350.

Hanuise, C., Villain, J.-P., Cerisier, J. C., Senior, C., Ruohoniemi, J. M., Greenwald, R. A., & Baker, K. B. (1991). Statistical study of high-latitude *E*-region Doppler spectra obtained with SHERPA HF radar. *Annales Geophysicae, 9*, 273–285.

Heinselman, C. J., & Nicolls, M. J. (2008). A Bayesian approach to electric field and *E*-region neutral wind estimation with the Poker Flat Advanced Modular Incoherent Scatter Radar. *Radio Science, 43*, RS5013. https://doi.org/10.1029/ 2007RS003805.

Koustov, A.V., Igarashi, K., Andre, D., Ohtaka, K., Sato, N., Yamagishi, H. & Yukimatu, A. (2001). Observations of 50-MHz and 12-MHz auroral coherent echoes at the Antarctic Syowa station. *Journal of Geophysical Research: Space Physics*, *106*, 12,875-12,887. https://doi.org/10.1029/2000JA000165.

Koustov, A. V., Danskin, D. W., Uspensky, M. V., Ogawa, T., Janhunen, P., Nishitani, N., Nozawa, S., Lester, M., & Milan, S. E. (2002). Velocities of auroral coherent echoes at 12 and 144 *Annales Geophysicae* MHz., *20*, 1647–1661. https://doi.org/10.5194/angeo-20-1647-2002.

Koustov, A. V., Danskin, D. W., Makarevitch, R. A., & Gorin, J. D. (2005). On the relationship between the velocity of *E*-region HF echoes and E × B plasma drift. *Annales Geophysicae, 23*, 371–378. https://doi.org/10.5194/angeo-23-371-2005.

Lacroix, P. J., & Moorcroft, D. R. (2001). Ion acoustic HF radar echoes at high latitudes and far ranges. *Journal of Geophysical Research: Space Physics*, *106*, 29091– 29103. https://doi.org/10.1029/2001JA000024.

Makarevitch, R. A., Koustov, A. V., Igarashi, K., Sato, N., Ogawa, T., Ohtaka, K., Yamagishi, H., & Yukimatu, A. S. (2002). Comparison of flow angle variations of *E*-region echo characteristics at VHF and HF. *Advances in Polar Upper Atmosphere Research, 16*, 59–83.

Makarevitch, R. A., Honary, F., & Koustov, A. V. (2004). Simultaneous HF measurements of *E*- and *F*-region Doppler velocities at large flow angles. *Annales Geophysicae, 22*, 1177–1185. https://doi.org/10.5194/angeo-22-1177-2004.

Makarevich, R. A. (2008). HF radar observations of high-velocity *E*-region echoes from the eastward auroral electrojet. *Journal of Geophysical Research: Space Physics*, *113*, A09321, https://doi.org/10.1029/2008JA013204.

Makarevich, R. A. (2009). Coherent radar measurements of the Doppler velocity in the auroral *E* region, *Radio Science Bulletin*, *327*, 33–46.

Makarevich, R. A. (2010). On the occurrence of high-velocity *E*-region echoes in SuperDARN observations. *Journal of Geophysical Research: Space Physics*, *115*, A07302. https://doi.org/10.1029/2009JA014698.

Milan, S. E., Yeoman, T. K., Lester, M., Thomas, E. C., & Jones, T. B. (1997). Initial backscatter occurrence statistics from the CUTLASS HF radars. *Annales Geophysicae*, *15*, 703-718. https://doi.org/10.1007/s00585-997-0703-0.

Milan, S. E., & Lester, M. (1998). Simultaneous observations at different altitudes of ionospheric backscatter in the eastward electrojet. *Annales Geophysicae*, *16*, 55-68. https://doi.org/10.1007/s00585-997-0055-9.

Milan, S. E., Lester, M., Yeoman, T. K., Robinson, T. R., Uspensky, M. V., & Villain, J.-P. (2004). HF radar observations of high-aspect angle backscatter from the *E*-region. *Annales Geophysicae*, *22*, 829–847. https://doi.org/10.5194/angeo-22-829-2004.

Nielsen, E. & Schlegel, K. (1985). Coherent radar Doppler measurements and their relationship to the ionospheric electron drift velocity. *Journal of Geophysical Research: Space Physics*, *90*, 3498-3504. https://doi.org/10.1029/JA090iA04p03498.

Nishitani, N., Ruohoniemi, J.M., Lester, M., Baker, J. B. H., Koustov, A.V., Shepherd, S.G., Chisham, G., Hori, T., Thomas, E.G., Makarevich, R.A., Marchaudon, A., Ponomarenko, P., Wild, J., Milan, S., Bristow, W.A., Devlin, J., Miller, E., Greenwald, R.A., Ogawa, T. & Kikuchi, T. (2019). Review of the accomplishments of mid-latitude SuperDARN HF radars. *Progress in Earth and Planetary Science*, *6*, *27*. https://doi.org/10.1186/s40645-019-0270-5.

Ponomarenko, P. V., St.-Maurice, J.-P., Waters, C. L., Gillies, R. G., & Koustov, A.V. (2009). Refractive index effects on the scatter volume location and Doppler velocity estimates of ionospheric HF backscatter echoes. *Annales Geophysicae*, *27*, 1-13. https://doi.org/10.5194/angeo-27-4207-2009.

Ponomarenko, P. V. (2013). SuperDARN velocity errors, Paper presented at SuperDARN Workshop, 26-31 May 2013, Moose Jaw, SK, Canada.

Ponomarenko P., St-Maurice J.-P., & McWilliams, K. A. (2018). Calibrating HF radar elevation angle measurements using E layer backscatter echoes. *Radio Science*, *53*, 1438– 1449. https://doi.org/10.1029/2018RS006638.

Reimer, A. S., Hussey, G. C., & McWilliams, K. A. (2018). Statistically self-consistent and accurate errors for SuperDARN data. Radio Science, 53, 93–111. https://doi.org/10.1002/2017RS006450.

Ruohoniemi, J. M., & Baker, K. B. (1998). Large-scale imaging of high-latitude convection with Super Dual Auroral Radar Network HF radar observations. *Journal of Geophysical Research: Space Physics*, *103*, 20797-20811. https://doi.org/10.1029/98JA01288.

Schlegel, K. (1996). Coherent backscatter from ionospheric E-region plasma irregularities. *Journal of Atmospheric and Solar Terrestrial Physics*, *58*, 933–941. https://doi.org/10.1016/0021-9169(95)00124-7.

Themens, D. R., Jayachandran, P. T, Galkin, I., & Hall, C. (2017). The Empirical Canadian High Arctic Ionospheric Model (E-CHAIM): N_mF_2 and h_mF_2. *Journal of Geophysical Research: Space Physics, 122*, 9015–9031. https://doi.org/10.1002/2017JA024398.

Shepherd, S. G. (2014). Altitude-adjusted corrected geomagnetic coordinates: Definition and functional approximations. *Journal of Geophysical Research: Space Physics*, *119*, 7501– 7521, doi:10.1002/2014JA020264.

Thomas, E. G., & Shepherd, S. G. (2018). Statistical patterns of ionospheric convection derived from mid-latitude, high-latitude, and polar SuperDARN HF radar observations. *Journal of Geophysical Research: Space Physics*, *123,* 3196–3216. https://doi.org/10.1002/2018JA025280.

Uspensky, M. V., Koustov, A. V., & Williams, P. J. S. (1993). The amplitude of auroral backscatter: III. Effect of tilted ionospheric layer. *Journal of Atmospheric and Terrestrial Physics*, *55*, 1383-1392. https://doi.org/10.1016/0021-9169(93)90106-9.

Uspensky, M. V., Kustov, A. V., Sofko, G. J., Koehler, J. A., Villain, J. P., Hanuise, C., Ruohoniemi, J. M., & Williams, P. J. S. (1994). Ionospheric refraction effects in slant range profiles of auroral HF coherent echoes. *Radio Science*, *29*, 503– 517, https://doi.org/10.1029/93RS03256.

Uspensky, M.V., Koustov, A. V., & Nozawa, S. (2006). STARE velocities at large flow angles: Is it related to the ion-acoustic speed? *Annales Geophysicae, 24*, 873-885. https://doi.org/10.5194/angeo-24-873-2006.

Uspensky, M.V., Koustov, A.V., Eglitis, P., Huuskonen, A., Milan, S.E., Pulkkinen, T., & Pirjola, R. (2001). CUTLASS HF radar observations of high-velocity *E*-region echoes. *Annales Geophysicae, 19*, 411-424. https://doi.org/10.5194/angeo-19-411-2001.

Yakymenko, K.N., Koustov, A. V., & Nishitani, N. (2015). Statistical study of midlatitude *E* region echoes observed by the Hokkaido SuperDARN HF radar. *Journal of Geophysical Research: Space Physics*, *120*, 9959–9976. https://doi.org/10.1002/2015JA021685.